Journal of Naval Architecture and Marine Engineering
December, 2018
https://doi.org/10.3329/jname.v15i2.31266 http://www.banglajol.info

LARGE EDDY SIMULATION OF TURBULENT CHANNEL FLOW USING DIFFERENTIAL EQUATION WALL MODEL

M. S. I. Mallik [1] and M. A. Uddin[2]

[1]Department of Arts and Sciences, Ahsanullah University of Science and Technology, Dhaka, Bangladesh, Email: saiful_math.as@aust.edu

[2]Department of Mathematics, Shahjalal University of Science and Technology, Sylhet, Bangladesh, Email: auddin-mat@sust.edu

Abstract:

A large eddy simulation (LES) of a plane turbulent channel flow is performed at a Reynolds number Re_τ = 590 based on the channel half width, δ and wall shear velocity, u_τ by approximating the near wall region using differential equation wall model (DEWM). The simulation is performed in a computational domain of $2\pi\delta \times 2\delta \times \pi\delta$. The computational domain is discretized by staggered grid system with $32 \times 30 \times 32$ grid points. In this domain the governing equations of LES are discretized spatially by second order finite difference formulation and for temporal discretization the third order low-storage Runge-Kutta method is used. Essential turbulence statistics of the computed flow field based on this LES approach are calculated and compared with the available Direct Numerical Simulation (DNS) and LES data where no wall model is used. Comparing the results throughout the calculation domain, it is found that the LES results based on DEWM show closer agreement with the DNS data, especially at the near wall region. That is, the LES approach based on DEWM can capture the effects of near wall structures more accurately. Flow structures in the computed flow field in the 3D turbulent channel have also been discussed and compared with LES data using no wall model.

Keywords: Large eddy simulation, differential equation wall model, standard Smagorinsky model, turbulent channel flow, staggered grid system.

NOMENCLATURE

x	streamwise direction
y	wall normal direction
z	spanwise direction
t	time
$\overline{u}_i$	filtered velocity component
u_i'	subgrid scale velocity component
$\overline{p}$	filtered pressure
C_S	Smagorinsky constant
u_τ	wall shear velocity
y^+	non-dimensional wall unit
Re_τ	flow Reynolds number
$\overline{S}_{ij}$	strain-rate tensor in the filtered field
A_{ij}	velocity gradient tensor
Q	second invariant of velocity gradient tensor

Greek symbols

Δ	filter width
Δx	grid spacing in streamwise direction
Δy	grid spacing in wall normal direction
Δz	grid spacing in spanwise direction
ν	kinematic viscosity
ν_S	subgrid scale eddy viscosity
ν_T	turbulent eddy viscosity
δ	channel half width
ρ	density of fluid
τ_{ij}	subgrid scale Reynolds stress
τ_x	streamwise shear stress
τ_{wi}	wall shear stress in ith direction
Ω_{ij}	Rotation tensor

1. Introduction

Turbulent wall-bounded flows are commonly encountered in engineering practice and are of considerable interests in a variety of industrial applications. For numerical simulations and validation of turbulent models,

1813-8235 (Print), 2070-8998 (Online) Received on: Jan 2017

turbulent wall-bounded flow or more specifically, turbulent channel flow is an important test case. Its geometry is simple and attractive for the researchers for both the experimental and computational studies on turbulent flow. Consequently, a broad range of experimental and computational studies of turbulent channel flow have been carried out (Dritselis, 2014; Elbatran, 2016; GrÖtzbach, 1987; Kim *et al.*, 1987; Mallik and Uddin, 2016; Mallik *et al.*, 2014; Moser *et al*., 1999; Schumann, 1975; Uddin and Mallik, 2015; Yang *et al.*, 2008).

Experimental evidence indicates that the larger scales of turbulence are flow-dependent, while the smaller ones are more universal. The larger scales are responsible for most of the production, convection, and redistribution of the energy, while the smaller ones are mainly responsible for the dissipation of the energy. These observations lead to the conclusion that LES, which resolves the large scales and models the small ones. For studying flows of practical interest the LES is currently the most promising method (Balaras *et al.*, 1996; Cabot, 1995; Cabot and Moin, 2000; Dritselis, 2014; GrÖtzbach, 1987; Mallik and Uddin, 2016; Mallik *et al.*, 2014; Sagaut, 2001; Uddin *et al.*, 2006; Uddin and Mallik, 2015; Xie *et al.*, 2013; Yang *et al.*, 2008). The position of LES is intermediate between DNS (GrÖtzbach, 1987; Mallik *et al.*, 2013; Moser *et al*., 1999) and Reynolds-averaged Navier-Stokes equations (RANS) techniques. Although DNS is considered as the exact approach to turbulence simulation, this simulation is very expensive for high Reynolds number case and requires large number of computational grids. On the other hand, the most used approximation to the solution of turbulent flow is RANS (Ferziger and Perić, 2002; Jagadeesh and Murali, 2005; Kianejad and Ansarifard, 2016), but this approach suffers from one principal shortcoming that the model used here must represent a very wide range of scales.

In the wall-bounded flows, the near wall region of the boundary layer needs to be directly resolved in LES with sufficiently fine resolution. This approach comes with very high computational cost. Another approach in LES for the wall-bounded flows is to model the near-wall dynamics by the wall stress models. The main advantage of this method is that the resolution requirement can be reduced significantly. There are several wall stress models to approximate the near wall region e.g. Schumann model (Schumann, 1975), GrÖtzbach model (GrÖtzbach, 1987), Algebraic wall model (Spalding, 1961), etc. Wall stress models based on boundary-layer approximations are more sophisticated stress model suggested by Balaras *et al.* (1996), Cabot (1995), Cabot and Moin (2000) and others. Such a model can capture the effects of near-wall structures more accurately. In these models, three-dimensional turbulent boundary layer (TBL) equations are solved numerically in a region in between the first off-wall grid points in LES and the wall to compute the wall shear stresses. These wall shear stresses are then forced at the outer boundary by the instantaneous tangential velocities from LES, while no-slip conditions are applied at the wall. The turbulent eddy viscosity can be obtained by a RANS type mixing-length eddy viscosity model. In this study, we approximated the near wall region by DEWM to capture the effects of near wall structures more accurately.

To perform LES in a turbulent channel flow, discretization method is another concern. Since the governing equations of LES are unsteady, to solve them numerically both space and time discretizations are needed. There are several discretization methods for spatial and temporal discretization of the governing equations of LES. For spatial discretization the conventional finite difference method (Ham *et al.*, 2002; Morinishi, 2010) is the most straightforward one. It is widely used with structured grids. For temporal discretization or equivalently in another word, for time integration explicit Runge-Kutta methods are a popular choice, and they are cheaper than implicit methods. Typical LES calculations demand minimum levels of memory locations during the time integration. In this case, low-storage Runge-Kutta scheme (Kennedy *et al.*, 2000; Williamson, 1980) is significant. Because, low-storage Runge-Kutta schemes require minimum levels of memory locations during the time integration and efficiently fulfill the modern large-scale scientific computing needs.

Therefore, the objective of this study is to perform LES of a plane turbulent channel flow with near wall region approximation by DEWM. The governing equations of LES are discretized by third order Low-Storage explicit Runge-Kutta method in time and second order finite difference formulation in space in a staggered grid system. For subgrid scale (SGS) modeling in LES the Standard Smagorinsky model is used. Essential turbulence statistics based on this approach are calculated and compared with DNS data of Moser *et al.* (1999) and LES data of Uddin and Mallik (2015). Instantaneous streamwise shear velocity distribution at the immediate vicinity of the wall and instantaneous streamwise velocity distribution at the centerline plane of the channel are also discussed by different contour plots and compared with those obtained by Uddin and Mallik (2015). Vortical structures using second invariant of velocity gradient tensor in the 3D turbulent channel flow are visualized and compared with that of Uddin and Mallik (2015). More specifically, the prime objective of this study is to investigate the performance of DEWM in LES.

2. Governing Equations

The governing equations of LES for an incompressible plane channel flow are the filtered Navier-Stokes and continuity equations for constant density in Cartesian co-ordinates given as

$$\frac{\partial \overline{u}_i}{\partial t}+\frac{\partial}{\partial x_j}\left(\overline{u}_i\,\overline{u}_j+\tau_{ij}\right)=-\frac{1}{\rho}\frac{\partial \overline{p}}{\partial x_i}+\frac{\partial}{\partial x_j}\left[\nu\left(\frac{\partial \overline{u}_i}{\partial x_j}+\frac{\partial \overline{u}_j}{\partial x_i}\right)\right], \text{ where } i, j = 1, 2, 3 \tag{1}$$

$$\frac{\partial \overline{u}_i}{\partial x_i}=0 \tag{2}$$

where the index i = 1, 2, 3 refers to the x, y and z directions respectively. Here $\overline{u}_x$, $\overline{u}_y$, $\overline{u}_z$ are streamwise, wall normal and spanwise filtered velocity respectively. ρ represents the fluid density, $\overline{p}$ is the filtered pressure and ν represents the kinematic viscosity. τ_{ij} is SGS Reynolds stress which is in fact the large scale momentum flux caused by the action of the small scales. The equations are non-dimensionalized by the channel half-width δ, and the wall shear velocity u_τ. The flow Reynolds number is therefore written as $Re_\tau = u_\tau \delta/\nu$. A schematic geometry of the plane channel flow and the co-ordinate system are shown in Fig. 1.

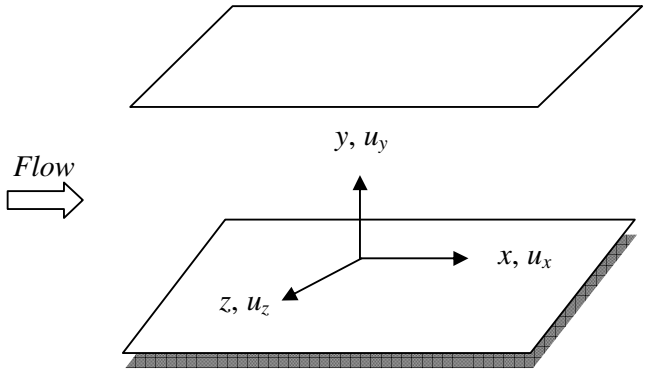

Fig. 1: Schematic geometry of plane channel flow.

In LES by applying a spatial filtering operation the velocity field u_i is decomposed into a filtered or large scale component $\overline{u}_i$ and a subgrid scale component u_i'. According to Sagaut (2001), this decomposition is represented as

$$u_i=\overline{u}_i+u_i' \tag{3}$$

The large scale or resolved velocity component $\overline{u}_i$ can be expressed as

$$\overline{u}_i\left(x_1,x_2,x_3,t\right)=\int_{-\infty}^{+\infty}\int_{-\infty}^{+\infty}\int_{-\infty}^{+\infty}\left(\prod_{i=1}^{3}G_i\left(x_i-x_i'\right)\right)u_i\left(x_1',x_2',x_3',t\right)dx_1'dx_2'dx_3' \tag{4}$$

where $G_i\left(x_i-x_i'\right)$ is a general filtering function which satisfies the following relation:

$$\int_{-\infty}^{+\infty}\int_{-\infty}^{+\infty}\int_{-\infty}^{+\infty}\left(\prod_{i=1}^{3}G_i\left(x_i-x_i'\right)\right)dx_1'dx_2'dx_3'=1 \tag{5}$$

In this approach the effect of the SGS field appears through the SGS Reynolds stress term, which is defined as

$$\tau_{ij} = \overline{u_i u_j} - \overline{u}_i \overline{u}_j \tag{6}$$

Experimental and numerical evidence indicates that the most significant effect of the SGS Reynolds stresses is to transfer energy from the large eddies to the SGS eddies. LES requires a model to represent the effects of the SGS field on the filtered field. The models used to approximate the SGS Reynolds stress are called SGS models. There are a number of SGS models. The most commonly used SGS model is the Standard Smagorinsky model (Smagorinsky, 1963), which assumes that the SGS Reynolds stress deviator tensor, τ_{ij} is proportional to the local strain rate tensor of the filtered field, $\overline{S}_{ij}$ as follows:

$$\tau_{ij} = -2 v_s \overline{S}_{ij} \tag{7}$$

The proportionality factor is the SGS eddy viscosity, v_S which is defined as

$$v_s = \left(C_s \Delta\right)^2 \left|\overline{S}\right| \tag{8}$$

The quantity C_S is the Smagorinsky constant which is not fixed for channel flows. Many authors used different values of C_S in LES. The value of this constant is, in practice, adjusted to improve the results. In this study, the simulation is performed for C_S = 0.065 in a plane channel. $\Delta = \left(\Delta x \Delta y \Delta z\right)^{1/3}$ is the filter width and $\left|\overline{S}\right| = \sqrt{2\overline{S}_{ij}\overline{S}_{ij}}$ is the magnitude of strain rate, where $\overline{S}_{ij} = \frac{1}{2}\left(\frac{\partial \overline{u}_i}{\partial x_j} + \frac{\partial \overline{u}_j}{\partial x_i}\right)$.

The presence of a solid wall modifies the turbulence dynamics in several ways. To represent the dynamics at the near-wall region correctly, it is important to modify the SGS models that verify the good properties in this region. This modification can be done by the introduction of Van-Driest damping function (Sagaut, 2001) in the SGS eddy viscosity. The SGS eddy viscosity is then modified as

$$v_s = \left(C_s f_s \Delta\right)^2 \left|\overline{S}\right| \tag{9}$$

Here $f_S = 1 - \exp\left(-\frac{y^+}{A^+}\right)$ is the Van-Driest damping function that has long been used for the reduced growth of the small scales near the wall, where y^+ is the distance from the wall in viscous wall units defined as $y^+ = \frac{y u_\tau}{v}$ and A^+ is a constant usually taken to be approximately 25 (Sagaut, 2001).

3. Numerical Methods and Grid System

The governing equations of LES are discretized by using the second order finite difference formulation in space and the third order low-storage explicit Runge-Kutta method in time (Kennedy *et al.*, 2000). The coupling between continuity equation and pressure fields is achieved by the simplified marker-and-cell (SMAC) method (Johnson *et al.*, 1994). Poisson equation for pressure is solved iteratively by a Preconditioned Incomplete Cholesky Decomposition Conjugated Gradient method. To approximate the near wall region the unsteady thin boundary layer equations are solved in this region by using the second order Adams-Bashforth scheme in time and second order finite difference formulation in space.

To discretize the governing equations of LES in space, the continuous space should be divided by a set of grid points. There are several types of computational grids. Among them the structured grids are commonly used. Conventional numerical algorithms based on structured grids mostly fall into three classes: regular, staggered

and collocated grid systems. In the regular grid system, the velocity components and pressure are stored at the same points. In collocated grid system, all variables are computed at the same location. This location corresponds to the cell center rather than a grid point at a cell vertex. In the Staggered grid approach, the location at which each independent variable is computed is different for all variables. This type of grid was introduced by Harlow and Welch (1965) in constructing Marker-and-cell (MAC) method. In particular, this type of grid is used for pressure correction methods. In this study we have used staggered grid system. Staggered grids may be constructed by several methods. An example of a staggered grid system in a two-dimensional plane is shown in our previous papers (Mallik *et al.*, 2014; Uddin and Mallik, 2015).

When the computational domain is discretized by the grid points, the governing equations should be discretized in this domain. Since the governing equations of LES are unsteady, to solve them numerically both spatial and temporal discretizations are required. For spatial discretization the second order finite difference formulation is widely used which is simply the substitution of the continuous differential operators with corresponding discrete operators, can be represented as (Morinishi, 2010):

$$\frac{\partial_1 \varphi}{\partial_1 x}\Big|_{i,j,k} = \frac{\varphi_{i,j,k} - \varphi_{i-1,j,k}}{\Delta x} \tag{10}$$

where φ is the discrete variable, Δx is grid spacing in x direction, and (i, j, k) denotes associated mesh indices in x, y and z directions. Subscript "1" indicates the stencil size. Discrete operators in the other directions are similarly defined. Second order differential operator is defined to be two successive applications of the first order operator. In addition to the discrete differencing operator we also define interpolation operators acting on different variables associated to the directions, which are given in our previous papers (Mallik *et al.*, 2014; Uddin and Mallik, 2015).

For temporal discretization or, for time integration of the governing equations of LES the low-storage explicit Runge-Kutta methods are a better choice. These methods generally have better stability properties and do not have a start-up problem. During the time integration the low-storage Runge-Kutta schemes require minimum levels of memory locations. As for example, the third order low-storage explicit Runge-Kutta scheme (Williamson, 1980) requires only two levels of memory locations during the time integration. Such a scheme is applied for the nonlinear convection and viscous terms in the governing equations, which is shortly described in our previous papers (Mallik *et al.*, 2014; Uddin and Mallik, 2015).

4. Computational Parameters

The computational domain of the mesh is selected to be $2\pi\delta \times 2\delta \times \pi\delta$ in streamwise, wall normal and spanwise directions respectively. The computation is performed in $32 \times 30 \times 32$ grid points which are distributed uniformly in the corresponding directions. In the computational domain the grid spacings in the streamwise, wall normal and spanwise directions are $\Delta x^+ \approx 116$, $\Delta z^+ \approx 58$ and $\Delta y^+ \approx 39.3$ wall units respectively. The superscript '+' indicates a non-dimensional quantity scaled by the wall variables; e.g. $y^+ = y u_\tau / \nu$, where $u_\tau = (\tau_w/\rho)^{1/2}$ is the wall shear velocity. The possible flow Reynolds number is $Re_\tau = 590$ which is based on δ and u_τ. The computation is carried out with a non-dimensional time increment, $\Delta t = 0.002$, which maintained a CFL number (Mallik *et al.*, 2014; Mallik and Uddin, 2016; Uddin and Mallik, 2015):

$$CFL = \Delta t \max\left(\frac{\left|\left\langle \overline{u}_x \right\rangle\right|}{\Delta x} + \frac{\left|\left\langle \overline{u}_y \right\rangle\right|}{\Delta y} + \frac{\left|\left\langle \overline{u}_z \right\rangle\right|}{\Delta z} \right) = 0.346 < 1.0 \tag{11}$$

where, $\left\langle \overline{u}_i \right\rangle$ denotes an ensemble average of $\overline{u}_i$. The computation is executed up to time, $t = n\Delta t$, where n is the number of time step.

In the LES calculation, the first off-wall grid points are at $y^+ \approx 19.7$ wall unit. At the region in between the first off-wall grid points in LES and the wall the unsteady thin boundary layer equations are solved. The grid numbers for this region computation are same as LES except in the direction normal to the wall, which is 34.

The grid points for this region approximation are distributed uniformly in the corresponding directions. In the wall normal direction, the grids coincide with the LES grids, and the grid spacing in this direction is $\Delta x_2^+ \approx 1.31$. A sample of grid generation in the given domain is shown in Fig. 2.

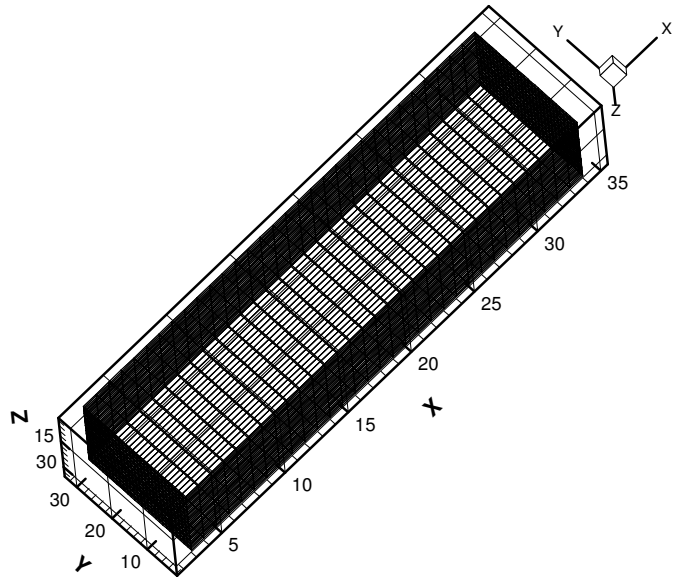

Fig. 2: A sample of grid generation in a plane channel.

5. Boundary Conditions

We consider fully developed incompressible viscous flow and use periodic boundary conditions in the streamwise and spanwise directions. The wall boundary condition is no-slip. For the staggered grid arrangement we set up additional nodes surrounding the physical boundary. The calculations are performed at internal nodes only. Just outside the solution domain the values of the velocity components are equated to the values of the nearest node just inside the solution domain (Versteeg and Malalasekera, 1995). The pressure boundary condition is periodic in the streamwise and spanwise directions. But in the wall normal direction the values of pressure, just outside the solution domain, are determined by assuming a zero gradient (Anderson, 1995).

6. Differential Equation Wall Model

Differential equation wall model is well established for separated flow regions and can capture the effects of near wall structures more accurately. In this model, the unsteady thin boundary layer equations which is in general are a simplified set of partial differential equations derived from the Navier-Stokes equations, are solved numerically at the near wall region in between the first off-wall grid points in LES and the wall. In this region the governing equations for horizontal velocity components U_i (i =1, 3) are (Cabot and Moin, 2000; Wang and Moin, 2002):

$$\frac{\partial U_i}{\partial t} + \frac{\partial}{\partial x_j}\left(U_i U_j\right) = -\frac{\partial P}{\partial x_i} + \frac{\partial}{\partial x_2}\left[\left(\nu + \nu_T\right)\frac{\partial U_i}{\partial x_2}\right] \tag{12}$$

with continuity

$$U_2 = -\int_0^{x_2}\left(\frac{\partial U_1}{\partial x_1} + \frac{\partial U_3}{\partial x_3}\right)dx_2 \tag{13}$$

where the index 1, 2, 3 refers to the streamwise, wall normal and spanwise directions respectively. The pressure P, in Eq. (12) is assumed x_2 – independent, equal to the value from the outer-flow LES solution. The turbulent eddy viscosity, ν_T can be obtained from a RANS type mixing-length eddy viscosity model with near-wall damping (Cabot, 1995; Cabot and Moin, 2000; Wang and Moin, 2002):

$$\frac{\nu_T}{\nu} = \kappa\, y_w^+ \left(1 - e^{-y_w^+/A}\right)^2 \tag{14}$$

where $y_w^+ = \dfrac{y_w u_\tau}{\nu}$ is the distance from the wall in wall units, κ is the model co-efficient, and A = 19. The boundary values of horizontal velocity components at the first off-wall grid points are obtained from the outer-flow LES velocity nodes and the wall boundary condition is no-slip. With those boundary conditions, Eqs. (12) and (13) are solved by using the second order Adams-Bashforth scheme in time and the second order finite difference formulae in space. Then, the wall shear stresses, τ_{wi} (i = 1, 3) are determined from the wall gradient of the solution:

$$\tau_{wi} = \nu \left.\frac{\partial U_i}{\partial x_2}\right|_{x_2 = 0} \tag{15}$$

Since the LES does not resolve the viscous sub-layer, approximate wall boundary conditions are imposed in terms of the wall shear stress components.

7. Grid Sensitivity Test

Grid sensitivity is the dependence of results upon the grid size. In the LES with no wall model (NWM) approximation the grid size in the streamwise and spanwise directions are uniform. But in the wall normal direction the computational grid is stretched by a hyperbolic tangent function:

$$Y(j) = \frac{\tanh\left[\gamma\left(\dfrac{2j}{N} - 1\right)\right]}{\tanh(\gamma)}, \quad j = 0,\ 1, \cdots\cdots, N, \tag{16}$$

where N is the number of grid points in that direction and γ is the stretching parameter, which is set to 2.25. In this direction, the minimum grid spacing is $\Delta y^+ \approx 2$ wall unit which exists at the immediate vicinity of the wall and maximum grid spacing is $\Delta y^+ \approx 42$ wall unit which exists at the centerline of the channel.

On the other hand, in the LES with DEWM approximation the region in between the first off-wall grid points in LES and the wall and the LES region are computed separately. For the approximation of the region in between the first off-wall grid points in LES and the wall the computational grid resolution is (32, 34, 32), and for the LES region approximation the computational grid resolution is (32, 30, 32) which are given in Section 4. The grid spacings in all directions for these two regions computation are uniform. Table 1 summarizes the number of grid points and grid spacings used in the given directions for different approximations in the same computational domain where the streamwise and spanwise directions are periodic.

Table 1: Comparison of grid points and grid spacings used in different approximations

Approximations	N_x	N_y	N_z	Δx^+	Δz^+	Δy^+ (center)
DNS	384	257	384	9.7	4.8	7.2
LES with NWM	32	64	32	116	58	42
LES with DEWM	32+32	34+30	32+32	116	58	1.31, 39.3

In this table, N_x, N_y and N_z denote the number of grid points used in the streamwise, wall normal and spanwise directions respectively. Here the grid spacing in the wall normal direction, Δy^+ is given at the channel centerline. At this position, $\Delta y^+ \approx 7.2$ for DNS calculation and $\Delta y^+ \approx 42$ for the LES with NWM approximation. Whereas, for the LES with DEWM approximation $\Delta y^+ \approx 1.31$ for the computation of the region in between the first off-wall grid points in LES and the wall, and $\Delta y^+ \approx 39.3$ for the LES region computation. Here, it is important to note that for the near wall region approximation denser grid points have

been used in the LES with DEWM approximation than that of the LES with NWM, and found that our present results show closer agreement with the DNS results in this region which one can be confirmed from Fig. 3 to Fig. 5.

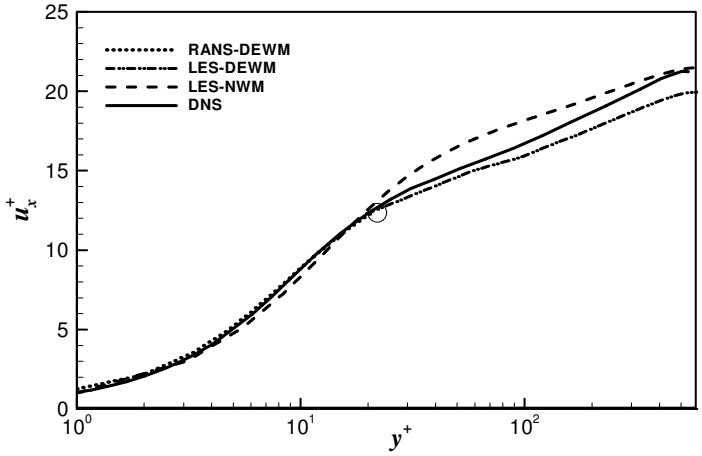

Fig. 3: The mean velocity profile in wall units.

The computations of our numerical code for the LES with NWM and LES with DEWM approaches were carried out on a computer equipped with Intel Core i5 Processor and 4GB of RAM. With this computer configuration the computational time for the LES with NWM approximation of Uddin and Mallik (2015) is approximately 6.50 CPU hours. On the other hand, for the LES with DEWM approximation the computational time is approximately 4.00 CPU hours. Hence, the computational time for the LES with DEWM approximation is smaller than that of LES with NWM.

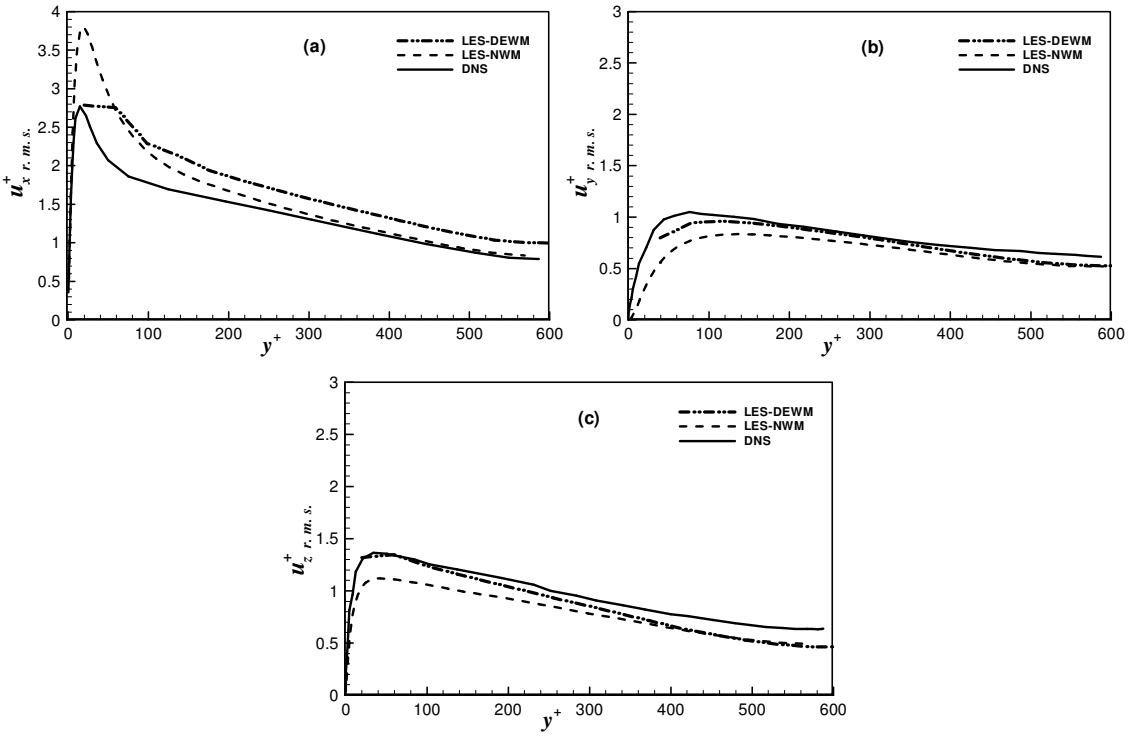

Fig. 4: Root mean square velocity profiles in wall units.

8. Validation of the Code

The computational model has been validated by comparing the present results with the results of Moser *et al*. (1999) and Uddin and Mallik (2015). Turbulence statistical results are compared with both those of Moser *et al*. (1999) and Uddin and Mallik (2015). But due to lack of availability of computational results for the turbulence flow structures in the given domain with the same Reynolds number, the flow structures obtained by the present results are compared with those of Uddin and Mallik (2015). The statistical results are presented from Fig. 3 to Fig. 5 and the flow structures are shown from Fig. 6 to Fig. 8. A sample of quantitative comparison in mean velocity profile for different approximations is given in Table 2 and found that the present results are in satisfactory agreement with the reported results.

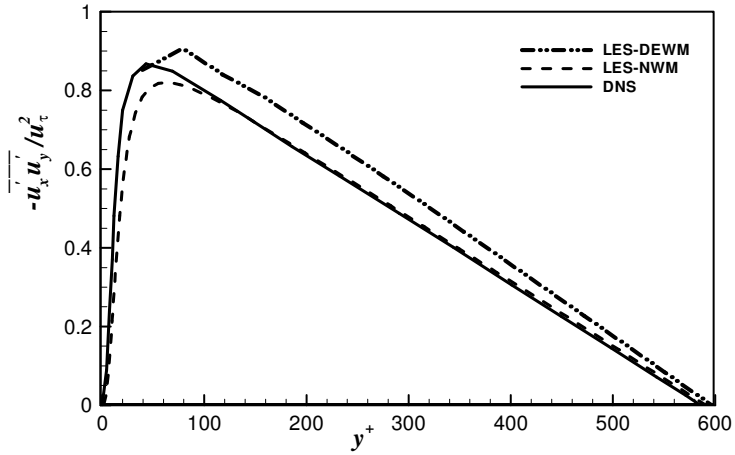

Fig. 5: The Reynolds stress profile in wall coordinates.

9. Results and Discussions

9.1 Turbulence statistics

This section discusses some essential statistics of the computed flow field in 3D turbulent channel flow corresponding to the channel half width. The statistical results are compared with the DNS data obtained by Moser *et al*. (1999) and LES data using no wall model (LES-NWM) of Uddin and Mallik (2015) which are represented by a solid and dashed line respectively in Figs. 3-5. In these figures, the calculated statistical results in the region in between the first off-wall grid points in LES and the wall are represented by a dotted line and the results calculated in rest of the region are indicated by a dash-dot-dot line. Furthermore, in this section a sample of quantitative comparison between the results of different simulations has also been shown. The simulations are initialized with a random solenoidal velocity field and integrated ahead in time with finite viscosity.

Numerous experiments have shown that the boundary layer in a plane turbulent channel flow can be divided into two parts: inner or near wall region and outer region. At the near wall region the dynamics is dominated by viscous effects, and in the outer region it is controlled by turbulence. Each of these regions can be split up into several layers corresponding to different types of dynamics. In the case of canonical boundary layer, the near wall region can be largely subdivided into three layers: viscous sub-layer ($y^+ \leq 5$), buffer layer ($5 < y^+ \leq 30$) and logarithmic inertial layer ($y^+ > 30$; $y/\delta << 1$) (Sagaut, 2001). The outer region includes the end of the logarithmic inertial layer and wake region.

The profiles of mean velocity normalized by the wall-shear velocity corresponding to the lower half of the channel for different approximations are shown in Fig. 3. The mean velocity is calculated by

$$u_x^+ = \frac{\langle \bar{u}_x \rangle}{u_\tau} \tag{17}$$

A circle shown in this figure indicates the interface between the RANS and LES regions which is located at about $y^+ \approx 19.7$. That is, the RANS region is defined as the viscous sub-layer and part of the buffer layer. The remaining region is defined as the LES region. In the RANS region, there is hardly noticeable difference between the three profiles. But here after in the LES region the computed velocity profile (LES-DEWM) under predicts the DNS profile, whereas, the LES-NWM profile is seen to be over predicted.

Table 2: Comparison between the results of mean velocity in different approximations

y^+	DNS	LES-NWM	RANS-DEWM & LES-DEWM
5.90	5.94	5.20	6.03
11.14	9.46	9.02	9.47
15.08	11.05	10.89	11.00
19.66	12.36	12.49	12.28
59.00	15.44	17.00	15.01
160.42	18.05	19.01	17.01
334.33	20.23	20.68	18.96
464.65	21.09	21.28	19.69

Table 2 provides a sample of the non-dimensional mean velocity at some positions of the channel in wall units which shows the quantitative comparison between the results of different approximations. From this table, it can be observed that the separation between the DNS and computed results (RANS-DEWM and LES-DEWM) increases with the increase of wall units. Using these data given in the table one can easily calculate relative errors in the LES results at the given positions. Percentage of relative errors generated in the results in the RANS region at a position $y^+ \approx 11.14$ for the LES approach based on DEWM is 0.10%, whereas for the LES-NWM approach it is 4.65%. After RANS region, in the LES region errors generated in the results at a position $y^+ \approx 160.42$ is 5.76% for the LES approach based on DEWM, whereas for the LES-NWM approach it is 5.32%. That is, in our approximation the error increases with the increase of wall units. But, at the near wall region our computed results show a good agreement with the DNS results. Therefore, the LES approach based on DEWM can capture the effects of near wall structures more accurately. In the error calculation the DNS data are considered as the true value, because DNS is considered as the exact approach to turbulence simulation.

The DNS and LES profiles of non-dimensional root mean square (*r.m.s.*) velocity components corresponding to the channel half width are displayed in Figs. 4(a), (b) and (c), which are defined as

$$u_x^+ \text{ r.m.s.} = \sqrt{\langle \bar{u}_x^2 \rangle - \langle \bar{u}_x \rangle^2} \Big/ u_\tau \tag{18}$$

$$u_y^+ \text{ r.m.s.} = \sqrt{\langle \bar{u}_y^2 \rangle - \langle \bar{u}_y \rangle^2} \Big/ u_\tau \tag{19}$$

$$u_z^+ \text{ r.m.s.} = \sqrt{\langle \bar{u}_z^2 \rangle - \langle \bar{u}_z \rangle^2} \Big/ u_\tau \tag{20}$$

Profiles of streamwise root mean square velocity for different approximations are shown in Fig. 4(a). This figure reveals that above the wall the LES profile based on DEWM starts with 2.78 near the peak value of DNS profile at the position $y+ \approx 19.98$. At this position the value for the LES-NWM approach is about 3.80. Beyond this position the trend of LES-DEWM profile is decreasing until the end of the range like the pattern of other two profiles.

Wall normal root mean square velocity profiles for the DNS and LES approaches are displayed in Fig. 4(b). From this figure it can be observed that at the near wall region from $y+ \approx 39.33$ to 180, the LES-DEWM profile under predicts the DNS profile. After that, from $y+ \approx 180$ to 350 the DNS and LES-DEWM profiles are almost collapsed. Finally, in rest of the range the LES-DEWM profile is seen to be under predicted. On the other hand, the wall normal root mean square velocity profile for the LES-NWM approach under predicts the DNS profile in the whole calculation domain. That is, the LES-DEWM profile shows less discrepancy from the DNS profile than that of the LES-NWM profile.

Profiles of spanwise root mean square velocity for different approximations are shown in Fig. 4(c). This figure reveals that there is hardly noticeable difference between the DNS and LES-DEWM profiles at the near wall region from $y+ \approx 19.67$ to 100. Whereas the LES-NWM profile under predicts the DNS profile. Here after in rest of the range both the LES profiles are seen to be under predicted. Hence, the LES-DEWM profile shows closer agreement with the DNS profile than that of the LES-NWM profile.

The profiles of non-dimensional Reynolds stress, $-\frac{\overline{u_x' u_y'}}{u_\tau^2}$ corresponding to the lower half of the channel for different approximations are shown in Fig. 5. When the flow reaches an equilibrium state then this profile becomes a straight line in a fully developed channel flow. Our computed results clearly indicate that case. From this figure it can be observed that above the wall the LES profile based on DEWM starts from near the peak value of DNS profile at the position $y+ \approx 39$. After this position, in rest of the range the LES-DEWM profile over predicts the DNS profile. It is also noticeable that the discrepancy of the LES-DEWM profile from the DNS and LES-NWM profiles decreases with the increase of the value of $y+$.

9.2 Flow structures

We have calculated streamwise velocity ($\overline{u}_x$) distribution at the centerline plane of the channel and streamwise shear velocity ($\overline{u}_{x\tau}$) distribution at the immediate vicinity of the wall at the end of calculation time when the flow reaches to an equilibrium state. Using these computed data different contour plots of the flow field have been drawn and compared with those obtained by Uddin and Mallik (2015).

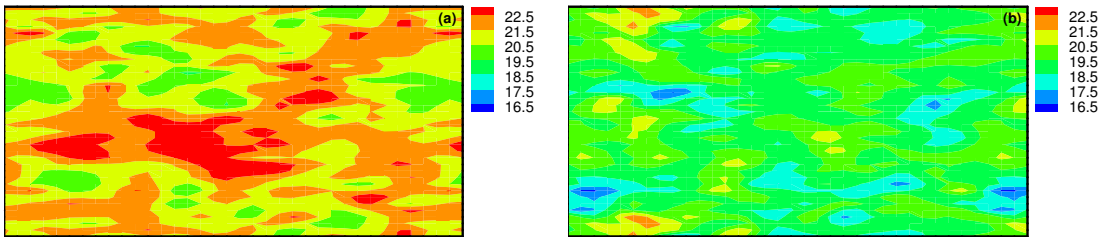

Fig. 6: Contours of streamwise velocity profiles in *x*-*z* plane for (a) LES using no wall model (Uddin and Mallik, 2015), and (b) LES using DEWM.

Contours of instantaneous streamwise velocity distribution at the centerline *x*-*z* plane of the channel for different LES approaches are shown in Figs. 6 (a) and (b). In these contour plots the values of $\overline{u}_x$ ranged between 16.5 and 22.5. The results in Fig. 7(a) were obtained by Uddin and Mallik (2015), where no wall model was used in LES, and Fig. 7(b) has been drawn by the LES data based on DEWM. In these figures, the highest value of $\overline{u}_x$ appears at red regions and lowest value at blue regions. In Fig. 6(a), the contribution of the larger values of $\overline{u}_x$ is more than that of the smaller values in the whole distribution. On the other hand, in Fig. 6(b) the contribution of the medium values of $\overline{u}_x$ is more located in the whole distribution. Therefore, the distinctive features of streamwise velocity in these contour plots are that the existence of the regions of larger values are more located in Fig. 6(a) than that in Fig. 6(b).

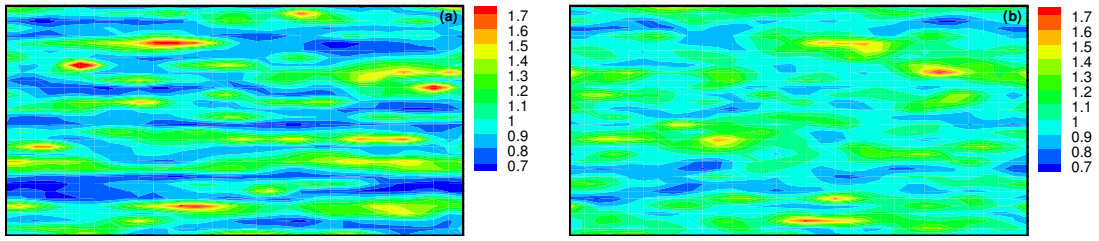

Fig. 7: Contours of streamwise shear velocity profiles in x-z plane for (a) LES using no wall model (Uddin and Mallik, 2015), and (b) LES using DEWM.

Contours of instantaneous streamwise shear velocity distribution at the immediate vicinity of the wall of this channel in x-z plane for different approximations are displayed in Figs. 7 (a) and (b). Streamwise shear velocity can be calculated by using Eq. (21).

$$\overline{u}_{x\tau} = \sqrt{\frac{\tau_x}{\rho}} \tag{21}$$

where, $\overline{u}_{x\tau}$ = streamwise shear velocity

ρ = density of the fluid

τ_x = streamwise shear stress.

In these contour plots, the values of $\overline{u}_{x\tau}$ ranged between 0.7 and 1.7. The lowest value is indicated by a blue color, while the highest value by a red color. The results in Fig. 7(a) are for the LES-NWM approach obtained by Uddin and Mallik (2015) and results in Fig. 7(b) are for the LES-DEWM approach. From these contour plots it can be observed that the larger values of $\overline{u}_{x\tau}$ appear more densely at scattered locations in the whole distribution in between the boundary and centerline of the plane. One of the distinctive features of streamwise shear velocity in these two figures are that the existence of the regions of smaller values are more located in Fig. 7(a) than that in Fig. 7(b).

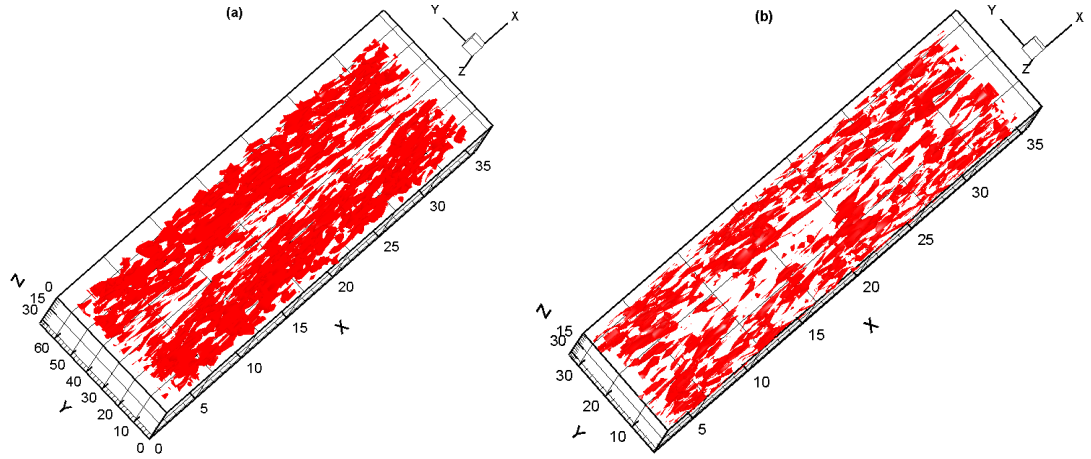

Fig. 8: Iso-surfaces of the second invariant (Q = 5) in the channel flow for (a) LES using no wall model (Uddin and Mallik, 2015), and (b) LES using DEWM.

Figs. 8(a) and (b) represent the visualization of vortical structures in the turbulent channel flow for different LES approaches. The vortical structures are visualized by iso-surfaces of the second invariant Q of velocity gradient tensor, which is defined as (Uddin *et al.*, 2006):

$$Q = -\frac{1}{2}\left(S_{ij}S_{ij} - \Omega_{ij}\Omega_{ij} \right) \tag{22}$$

$$\text{where, } S_{ij} = \frac{1}{2}\left(\frac{\partial \bar{u}_i}{\partial x_j} + \frac{\partial \bar{u}_j}{\partial x_i}\right) \text{ and } \Omega_{ij} = \frac{1}{2}\left(\frac{\partial \bar{u}_i}{\partial x_j} - \frac{\partial \bar{u}_j}{\partial x_i}\right) \tag{23}$$

are respectively, the strain-rate and rotation tensors, that is, the symmetric and asymmetric part of the velocity gradient tensor:

$$A_{ij} = \frac{\partial u_i}{\partial x_j} = S_{ij} + \Omega_{ij} \tag{24}$$

Since the velocity gradient tensor represents the balance between rotation and strain rate, flow visualization based on velocity gradient tensor can provide interesting evidence of direct linkage between inner and outer regions of the turbulent flow field. In these figures, the flow visualized region is the whole calculation domain. In Fig. 8(b) the near wall region is approximated by DEWM, but in Fig. 8(a) no wall model was used in LES. In both the figures the level of the iso-surfaces are selected to be $Q = 5$. For this value of Q the vortical structures are randomly distributed over the turbulent flow field. The vortices are generated more densely in between the boundary and central position of the channel than the ones generated around the central position of the channel. But, the density of vortical structures in Fig. 8(a) is more than that in Fig. 8(b).

10. Conclusions

A Large eddy simulation of a plane turbulent channel flow has been successfully carried out with $32\times30\times32$ grid points at a Reynolds number, 590 which is based on the channel half width and wall shear velocity. To capture the effects of near wall structures more accurately, the near wall region has been approximated by DEWM without taking sufficiently fine resolution. The DEWM lead to a significant reduction in the number of computational cells in this simulation. In spite of resolution limitations, the simulations are able to resolve the essential features of the statistical fields. The statistical results are compared with the DNS and LES data of reference. In comparison with the DNS data, the LES results based on DEWM show better agreement than that of the LES results using no wall model, especially at the near wall region. Instantaneous streamwise velocity distribution at the centerline x-z plane and instantaneous streamwise shear velocity distribution at the immediate vicinity of the wall of this channel have also been measured in the contour plots, and compared these contour plots with the LES results where no wall model was used. In these contour plots, one of the distinctive features in streamwise velocity and streamwise shear velocity distributions are that the existence of the regions of larger values of streamwise velocity are more located for the LES-NWM approach than that of LES-DEWM, and the existence of the regions of smaller values of streamwise shear velocity are less located for the LES-DEWM approach than that of LES-NWM. In the computed flow field the vortical structures are visualized by iso-surfaces of the second invariant of velocity gradient tensor, and compared with that of the LES-NWM approach. The flow field contains lots of tube-like vortical structures which are significant and randomly distributed over the turbulent flow field. Compared with LES-NWM approach, in this simulation the vortices are generated less densely.

Acknowledgements

This research work is partially supported by the ‘Bangabandhu Fellowship on Science and ICT Project’ which is gratefully acknowledged.

References

Anderson, Jr. J. D. (1995): Computational Fluid Dynamics, McGraw-Hill, New York.

Balaras, E., Benocci, C. and Piomelli, U. (1996): Two-layer approximate boundary conditions for large-eddy simulations, AIAA Journal, Vol. 34, No. 6, pp. 1111-1119. https://doi.org/10.2514/3.13200

Cabot, W. (1995): Large-eddy simulations with wall models, Annual Research Briefs, Center for Turbulence Research, Stanford University, CA, pp. 41-50.

Cabot, W. and Moin, P. (2000): Approximate wall boundary conditions in the large-eddy simulation of high Reynolds number flow, Journal of Flow, Turbulence and Combustion, Vol. 63, pp. 269-291. https://doi.org/10.1023/A:1009958917113

Dritselis, C. D. (2014): Large eddy simulation of turbulent channel flow with transverse roughness elements on one wall, International Journal of Heat and Fluid Flow, Vol. 50, pp. 225-239. https://doi.org/10.1016/j.ijheatfluidflow.2014.08.008

Elbatran, A. H. (2016): DES of the turbulent flow around a circular cylinder of finite height, Journal of Naval Architecture and Marine Engineering, Vol. 13, pp. 179-188. https://doi.org/10.3329/jname.v13i2.29994

Ferziger, J. H. and Perić, M. (2002): Computational Methods for Fluid Dynamics, Springer-Verlag, Berlin. https://doi.org/10.1007/978-3-642-56026-2

Grötzbach, G. (1987): Direct numerical and large eddy simulation of turbulent channel flows, Encyclopedia of Fluid Mechanics, Cheremisinoff, N. P. ed., Gulf Pub. Co., Chap. 34, pp. 1337-1391.

Ham, F. E., Lien, F. S. and Strong, A. B. (2002): A Fully conservative second-order finite difference scheme for incompressible flow on nonuniform grids, Journal of Computational Physics, Vol. 177, pp. 117-133. https://doi.org/10.1006/jcph.2002.7006

Harlow, F. H. and Welch, J. E. (1965): Numerical calculation of time-dependent viscous incompressible flow with free surface, Physics of Fluids, Vol. 8, No. 12, pp. 2182-2189. https://doi.org/10.1063/1.1761178

Jagadeesh, P. and Murali, K. (2005): Application of low-Re turbulence models for flow simulations past underwater vehicle hull forms, Journal of Naval Architecture and Marine Engineering, Vol. 2, pp. 41-54. https://doi.org/10.3329/jname.v2i1.2029

Johnson, D. B., Raad, P. E. and Chen, S. (1994): Simulation of impacts of fluid free surfaces with solid boundaries, International Journal for Numerical Methods in Fluids, Vol. 19, No. 2, pp. 153-176. https://doi.org/10.1002/fld.1650190205

Kennedy, C. A., Carpenter, M. H. and Lewis, R. M. (2000): Low-storage, explicit Runge-Kutta schemes for the compressible Navier-Stokes equations, Applied Numerical Mathematics, Vol. 35, pp. 177-219. https://doi.org/10.1016/S0168-9274(99)00141-5

Kianejad, S.S. and Ansarifard, N. (2016): Numerical simulation of turbulent boundary layers of surfaces covered with foul release and antifouling coatings, Journal of Naval Architecture and Marine Engineering, Vol. 13, pp. 17-26. https://doi.org/10.3329/jname.v13i1.26017

Kim, J., Moin, P. and Moser, R. (1987): Turbulence statistics in fully developed channel flow at low Reynolds number, Journal of Fluid Mechanics, Vol. 177, pp. 133-166. https://doi.org/10.1017/S0022112087000892

Mallik, M. S. I. and Uddin, M. A. (2016): Large eddy simulation of turbulent channel flow using algebraic wall model, Journal of Korean Society for Industrial and Applied Mathematics, Vol. 20, No. 1, pp. 37-50. https://doi.org/10.12941/jksiam.2016.20.037

Mallik, M. S. I., Uddin, M. A. and Meah, M. A. (2014): Large eddy simulation of turbulent channel flow at Re_τ= 590, IOSR – Journal of Mathematics, Vol. 10, No. 6, pp. 41-50. https://doi.org/10.9790/5728-10644150

Mallik, M. S. I., Uddin, M. A. and Rahman, M. A. (2013): Direct numerical simulation in two dimensional homogeneous isotropic turbulence using spectral method, Journal of Scientific Research, Vol. 5, No. 3, pp. 435-445. https://doi.org/10.3329/jsr.v5i3.12665

Morinishi, Y. (2010): Skew-symmetric form of convective terms and fully conservative finite difference schemes for variable density low-Mach number flows, Journal of Computational Physics, Vol. 229, pp. 276-300. https://doi.org/10.1016/j.jcp.2009.09.021

Moser, R. D., Kim, J. and Mansour, N. N. (1999): Direct numrical simulation of turbulent channel flow up to Reτ = 590, Physics of Fluids, Vol. 11, No. 4, pp. 943-945. https://doi.org/10.1063/1.869966

Sagaut, P. (2001): Large Eddy Simulation for Incompressible Flows: An Introduction, Springer-Verlag, Berlin. https://doi.org/10.1007/978-3-662-04416-2

Sanderse, B. and Koren, B. (2012): Accuracy analysis of explicit Runge-Kutta methods applied to the incompressible Navier-Stokes equations, Journal of Computational Physics, Vol. 231, No.8, pp. 3041-3063. https://doi.org/10.1016/j.jcp.2011.11.028

Schumann, U. (1975): Subgrid scale model for finite difference simulations of turbulent flows in plane channels and annuli, Journal of Computational Physics, Vol. 18, pp. 376-404. https://doi.org/10.1016/0021-9991(75)90093-5

Smagorinsky, J. (1963): General circulation experiments with the primitive equations. I: The basic experiment, Monthly Weather Review, Vol. 91, No. 3, pp. 99-165. https://doi.org/10.1175/1520-0493(1963)091<0099:GCEWTP>2.3.CO;2

Spalding, D. B. (1961): A single formula for the law of the wall, Journal of Applied Mechanics, Vol. 28, No. 3, Ser. E, pp. 455-458. https://doi.org/10.1115/1.3641728

Uddin, A., Kato, C., Yamade, Y., Ohshima, N., Tanahashi, M. and Miyauchi, T. (2006): Large eddy simulation of homogeneous isotropic turbulent flow using the finite element method, JSME International Journal, Ser. B, Vol. 49, No. 1, pp. 102-114.

Uddin, M. A. and Mallik, M. S. I. (2015): Large eddy simulation of turbulent channel flow using Smagorinsky model and effects of Smagorinsky constants, British Journal of Mathematics & Computer Science, Vol. 7, No. 5, pp. 375-390. https://doi.org/10.9734/BJMCS/2015/15962

Versteeg, H. K. and Malalasekera, W. (1995): An Introduction to Computational Fluid Dynamics, Longman Group Limited, England.

Wang, M and P. Moin, P. (2002): Dynamic wall modeling for large-eddy simulation of complex turbulent flows, Physics of Fluids, Vol. 14, No. 7, pp. 2043-2051. https://doi.org/10.1063/1.1476668

Williamson, J. H. (1980): Low-storage Runge-Kutta schemes, Journal of Computational Physics, Vol. 35, pp. 48-56. https://doi.org/10.1016/0021-9991(80)90033-9

Xie, Z., Lin, B. and Falconer, R. A. (2013): Large-eddy simulation of the turbulent structure in compound open-channel flows, Advances in Water Resources, Vol. 53, pp. 66-75. https://doi.org/10.1016/j.advwatres.2012.10.009

Yang, F., Zhang, H. Q., Chan, C. K. and Wang, X. L. (2008): Large eddy simulation of turbulent channel flow with 3d roughness using a roughness element model, Chinese Physics Letters, Vol. 25, No. 1, pp. 191-194. https://doi.org/10.1088/0256-307X/25/1/052